Single-pixel coherent diffraction imaging

Kanghee Lee and Jaewook Ahn[a)]
Department of Physics, KAIST, Daejeon 305-701, Republic of Korea

(Received 27 July 2010; accepted 13 September 2010; published online 13 December 2010)

We demonstrate single-pixel coherent diffraction imaging, whereby broadband terahertz waveforms passed through a slanted phase retarder (SPR), diffracted from an object, were measured by a terahertz detector located in the far field. For one dimensional imaging, the fixed-location single-pixel broadband detector simultaneously measured all the spatial frequency components of the object because the frequency components of the source maintain a one-to-one correspondence with the object's spatial frequency. For two dimensional imaging, the angular position of the SPR enabled the diffracted terahertz wave to carry an angular projection image of the object. © *2010 American Institute of Physics*. [doi:10.1063/1.3525583]

Coherent diffraction imaging (CDI) is an image reconstruction technique for small-size objects using highly coherent optical, x-ray, or electron beams, in which a real-space image is reconstructed from a diffraction pattern collected by a detector array.[1] Newly developed high-energy photon sources permit CDI of nanoscale structures, such as nanotubes, quantum dots, and possibly proteins.[2–4] Also, CDI with optical waves has proven useful in obtaining tomographic high-resolution images of live cells.[5] The image resolution of CDI depends on the wavelength and the extension of the measured diffraction pattern. For a monochromatic wave of wavelength λ, the Fraunhoffer diffraction pattern $V(x)$ of an object $U(\xi)$ is

$$V(x) = \frac{e^{ikz}e^{i(kx^2/2z)}}{i\lambda z}\int U(\xi)e^{-i(2\pi/\lambda z)x\xi}d\xi, \tag{1}$$

where ξ and x represent spatial coordinates in the real and reciprocal spaces, respectively, k is the wave number, and z is the distance from the object to the detector. The Fourier component of $U(\xi)$ evaluated at spatial frequency $f_x(=x/\lambda z)$, that is, $\tilde{U}(f_x)$, is captured in $V(x)$, aside from the given phase factor. For a high-resolution image of maximum spatial frequency $f_{\max}$, an array detector of lateral size $x_{\max} = \lambda z/f_{\max}$ is required.

However, given a broadband coherent source with a frequency distribution ranging from zero to $\omega_{\max}/2\pi$, a single-point detector can replace the detector array because the frequency components of the source maintain a one-to-one correspondence with the spatial frequency components of the object. The point detector placed in a fixed position x_o can simultaneously measure all the Fourier components of $U(\xi)$; therefore, single-pixel imaging can be achieved such that

$$U(\xi) = \int_0^{\omega_{\max}} \tilde{U}(f_{x_o};\omega)e^{-i\xi f_{x_o}(\omega)}d\omega, \tag{2}$$

where ω is the angular frequency and $\omega_{\max}=2\pi c f_{\max}z/x_o$. In this proposed method for single-pixel coherent diffraction imaging (SP-CDI), the spatial resolution is limited by the frequency maximum $\omega_{\max}$ of the coherent source, not by the detector size.

For a broadband coherent source, we consider ultrafast terahertz pulses.[6] A typical terahertz pulse frequency range for terahertz time-domain spectroscopy (TDS) is 0–3 THz (Ref. 7) and a record broad bandwidth of 80 THz has been reported.[8] Conventional use of ultrafast terahertz waves in imaging involves a raster scan to move an object around a tightly focused terahertz beam[9] and this method has a diverse range of imaging applications extending from semiconductors and metal structures to biological and medical objects.[10–12] However, due to the limitation of the data acquisition speed of this mechanical scanning method, various alternatives have been proposed, including two dimensional (2D) electro-optic imaging,[13] a focal-plane detector array,[14] and compressed sensing techniques,[15] at the cost of implementation complexity. In our previous work, we demonstrated coherent optical computation for single-point terahertz imaging, where an active Fourier mask in a conventional terahertz-TDS setup converted a 2D image into N temporal waveforms.[16] In this letter, using a completely different approach, we propose single-pixel detection of coherent diffraction images and demonstrate various 2D image reconstructions.

In SP-CDI, a target 2D object is placed in the object plane $\Sigma_o(\xi,\eta)$, as shown in Fig. 1(a), and illuminated by

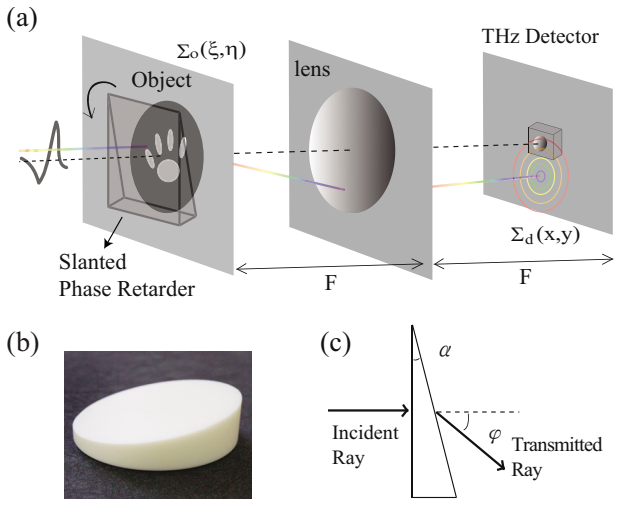

FIG. 1. (Color online) (a) Schematic of single-pixel coherent diffraction imaging. (b) Slanted phase retarder. (c) Illustration of beam deviation.

[a)]Electronic mail: jwahn@kaist.ac.kr.

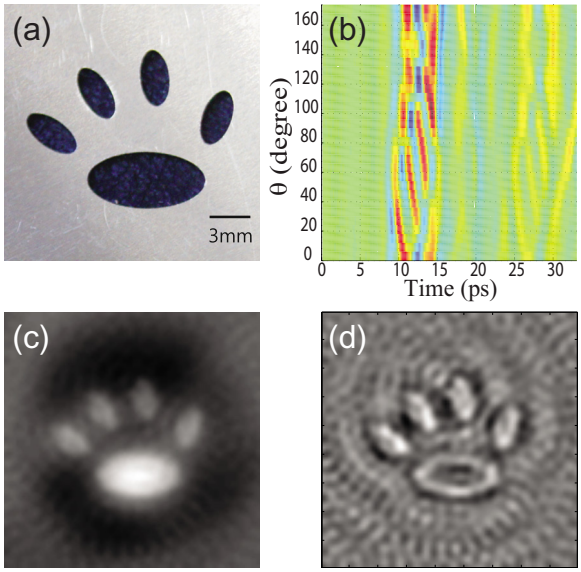

FIG. 2. (Color online) (a) Image target, a representation of a feline paw (size=2×2 cm^2). (b) Measured terahertz waveforms. (c) Reconstructed image. (d) Sharpened image by high-frequency filtering of measured waveforms in (b).

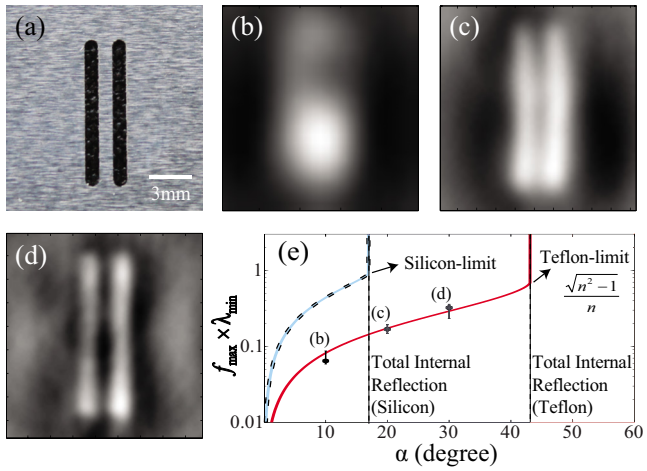

FIG. 3. (Color online) (a) Image resolution target consisting of 1 mm double slits separated by 2 mm. [(b)–(d)] Recovered images obtained using phase retarders slanted at angles $\alpha=10°$, 20°, and 30°, respectively. (e) Maximum spatial frequency f_{max} (in λ_{min} unit) plotted as a function of SPR angle α. [Solid line: Teflon, dashed line: silicon, and dots: measurements from (b)–(d).]

collimated terahertz waves. The diffracted field from the object $U(x,y)$ is then collected by a terahertz detector located at the center of the far-field diffraction plane $\Sigma_d(x,y)$, i.e., $x=y=0$. To redirect all the spatial frequency components to the detector location, a slanted phase retarder (SPR), shown in Fig. 1(b), is inserted in front of the object. For an incident terahertz wave of spectral field profile $S(\omega)$, the diffracted field $V_\theta(\omega)$ is given by

$$\frac{V_\theta(\omega)}{S(\omega)} = \frac{e^{ikz}}{i\lambda z}\int_{\Sigma_o} U(\xi,\eta)e^{ik(\xi\cos\theta+\eta\sin\theta)\sin\phi}d\xi d\eta, \qquad (3)$$

where θ is the angular position of the SPR and ϕ denotes the deviation angle of the beam through the SPR, as shown in Fig. 1(c). Due to the angular orientation of the SPR, the diffracted terahertz wave carries an angular projection image of the object. Using a procedure that is mathematically similar to the method described in Ref. 16, the original object $U(\xi,\eta)$ is recovered from a number of measurements carried out at different θ's by

$$U(\xi,\eta) \propto \mathcal{R}_\theta^{-1}\left\{\mathcal{F}^{-1}\left[\frac{V_\theta(\omega)}{\omega e^{ikz}S(\omega)}\right]\right\}, \qquad (4)$$

where $\mathcal{R}_\theta^{-1}$ and $\mathcal{F}^{-1}$ are the inverse Radon and inverse Fourier transformations, respectively.

For the experiment, we used a Ti:sapphire laser oscillator that produced IR short pulses at an average power of 350 mW. Terahertz waves were generated from a large-area photoconductive antenna[17] and then collimated by an off-axis parabolic mirror with a 150 mm focal length. For detecting the diffracted terahertz waves, a 2-mm-thick ZnTe electro-optic crystal was placed in the front focal plane of another parabolic mirror with a focal length of 100 mm. Time-resolved terahertz electric field measurements were carried out by mapping the polarization changes of optical gate beams.[18] The object, a representation of a feline paw shown in Fig. 2(a), was made from a 1-mm-thick metal plate with an area of 2×2 cm^2. The SPR was made out of polytetrafluoroethylene (Teflon) and had a cylindrical shape (radius of 25 mm) cut at an angle $\alpha=15°$. The index of refraction of Teflon is a constant $n=1.46$ over the terahertz spectral range. The procedure for data collection and image recovery was as follows. First, both the object and the SPR were temporarily removed and the reference terahertz field spectrum at the detector, $S_d(\omega)$, was obtained by taking the Fourier transform of a terahertz time-domain signal. We note that $S_d(\omega)$ differs from the terahertz field spectrum at the object by a factor of ω, aside from a constant factor. Then, the object and the SPR were replaced and $N=30$ different terahertz waveforms were measured at various angles uniformly sampled from $\theta=0°-180°$ [Fig. 2(b)]. The time-domain waveforms were recorded with a spectrum of up to $\omega_{max}=1.5$ THz with a resolution of 0.03 THz. By following the signal processing described in Eqs. (3) and (4), the coherent diffraction image was completely retrieved [Fig. 2(c)]. Owing to the one-to-one correspondence of the terahertz frequency to the image spatial frequency, the Fourier synthetic image processing can be implemented by directly manipulating the Fourier components of the terahertz waveforms. For example, a sharpened image, such as that in Fig. 2(d), was obtained via high-pass filtering of measured terahertz waveforms.

The SP-CDI image resolution is not directly related to the numerical aperture or the focal length of the diffractive optic. Instead, the beam deviation angle ϕ is a scaling coefficient between f_{max} and ω_{max}, i.e., $f_{max}=\omega_{max}\sin\phi/2\pi c$, and therefore determines the image resolution. Figure 3 shows the result of an imaging experiment with an object of a double-slit pattern. For 1 mm hole double slits separated by 2 mm, as shown in Fig. 3(a), three different SPRs cut at $\alpha=10°$, 20°, and 30° were used, and the diffraction images shown in Figs. 3(b)–3(d), respectively, were obtained. The SPR angles were chosen to give image resolutions of $1/f_{max}=2.4$, 1.2, and 0.7 mm, respectively, and as expected, the double-slit patterns were resolved in Figs. 3(c) and 3(d) only. For enhanced image resolution, larger SPR angles should be considered. However, from the relationship $\phi=\sin^{-1}(n\sin\alpha)-\alpha$, total internal reflection will occur in the SPR and the image resolution is limited as

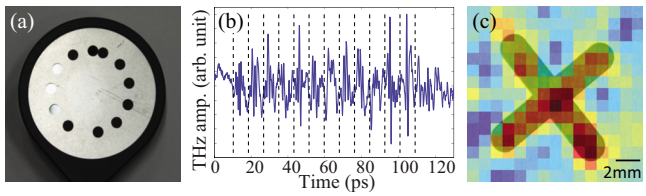

FIG. 4. (Color online) (a) The passive Fourier mask used for single-waveform 2D imaging. (b) Measured terahertz waveform. (c) Recovered image overlayed with the object (X-mark shade).

$$\frac{1}{f_{\max}} = \frac{\lambda_{\min}}{\sin\phi} \leq \frac{n}{\sqrt{n^2-1}}\lambda_{\min}, \tag{5}$$

where $\lambda_{\min}$ is the minimal wavelength of the given terahertz pulse. Figure 3(e) compares the measured maximal frequencies with Eq. (5): The calculated $f_{\max}$ from the images are shown in dots and the result from Eq. (5) in a solid line. Both, plotted as a function of the SPR angle α, show a good agreement. As a result, the resolution in SP-CDI is given by a function of both the index of refraction of the SPR and the maximal terahertz frequency, and the minimum $\lambda_{\min}$ is diffraction-limited for the same reason in optical microscopy.

It is worth noting that both the imaging methods in this work and Ref. 16 used *active masking*. The former used a real-domain filter and the latter a Fourier-domain filter. Both methods require the measurement of N different waveforms, each containing specific angular projection information of the object. Mathematically there exist a number of techniques that permit the extraction of complete spatial information for a 2D object from a single waveform.[19] The simplest method is the use of a single Fourier-domain mask [Fig. 4(a)] constructed with N holes of various phase retardations. This Fourier mask, used in a coherent computational setup in Ref. 16, temporally separates N terahertz waveforms, each containing individual angular object information with respect to each other. Then, a single time-domain scan of the diffracted terahertz wave, as shown in Fig. 4(b), simultaneously records the complete angular projection image of the 2D object, and therefore, a 2D image recovery from a single terahertz waveform is achieved, as shown in Fig. 4(c).

Our proposed idea eliminates the need for area detection in coherent diffraction imaging, and an array detection further allows fast and intelligent capture of certain features of a sample. Furthermore, SP-CDI can be implemented using broadband waves in different frequency ranges. For example, subfemtosecond pulses produced via high harmonic generation of an ultrashort infrared pulse in atoms encompass the whole spectral range of visible and UV/XUV.[20] Another candidate is the supercontinuum formed as a result of cascading nonlinear processes of IR short pulses, as seen, for example, in a photonic bandgap fiber, which spans several optical octaves with a spectral range extending from UV to beyond mid-IR.[21] Both broadband sources are capable of SP-CDI. In microscopic applications with optical and EUV sources, our technique promises phase-contrast imaging, three dimensional imaging, and Fourier synthetic imaging for many applications in medicine, biology, and material sciences.

In conclusion, we demonstrated coherent diffraction imaging using a fixed-location single-pixel detector. The broadband nature of the terahertz waves was used for one-to-one mapping of the spatial frequency of an object to the frequency of the diffracted waves, and by adopting a slanted phase retarder, a fixed-point single detector collected complete 2D angular projection images of various objects, enabling single-pixel 2D coherent diffraction imaging.

This work was supported by the Mid-career Researcher Program through the National Research Foundation of Korea (NRF) funded by the Ministry of Education, Science and Technology (Grant No. 2010-0013899).

[1] J. R. Fienup, Opt. Lett. **3**, 27 (1978).
[2] J. M. Zuo, I. Vartanyants, M. Gao, R. Zhang, and L. A. Nagahara, Science **300**, 1419 (2003).
[3] I. A. Vartanyants, I. K. Robinson, J. D. Onken, M. A. Pfeifer, G. J. Williams, F. Pfeiffer, H. Metzger, Z. Zhong, and G. Bauer, Phys. Rev. B **71**, 245302 (2005).
[4] R. Neutze, R. Wouts, D. Spoel, E. Weckert, and J. Hajdu, Nature (London) **406**, 752 (2000).
[5] Y. Sung, W. Choi, C. Fang-Yen, K. Badizadegan, R. R. Dasari, and M. S. Feld, Opt. Express **17**, 266 (2009).
[6] B. I. Greene, J. F. Federici, D. R. Dykaar, R. R. Jones, and P. H. Bucksbaum, Appl. Phys. Lett. **59**, 893 (1991).
[7] C. Fattinger and D. Grischkowsky, Appl. Phys. Lett. **54**, 490 (1989).
[8] T. Zentgraf, R. Huber, N. C. Nielsen, D. S. Chemla, and R. A. Kaindl, Opt. Express **15**, 5775 (2007).
[9] B. B. Hu and M. C. Nuss, Opt. Lett. **20**, 1716 (1995).
[10] D. M. Mittleman, M. Gupta, R. Neelamani, R. G. Baraniuk, J. V. Rudd, and M. Koch, Appl. Phys. B: Lasers Opt. **68**, 1085 (1999).
[11] M. T. Reiten, D. Grischkowsky, and R. A. Cheville, Appl. Phys. Lett. **78**, 1146 (2001).
[12] S. Wang, B. Ferguson, D. Abbott, and X. C. Zhang, J. Biol. Phys. **29**, 247 (2003).
[13] Q. Wu, T. D. Hewitt, and X.-C. Zhang, Appl. Phys. Lett. **69**, 1026 (1996).
[14] B. Pradarutti, R. Muller, W. Freese, G. Matthäus, S. Riehemann, G. Notni, S. Nolte, and A. Tünnermann, Opt. Express **16**, 18443 (2008).
[15] W. L. Chan, K. Charan, D. Takhar, K. F. Kelly, R. G. Baraniuk, and D. M. Mittleman, Appl. Phys. Lett. **93**, 121105 (2008).
[16] K. Lee, K. H. Jin, J. C. Ye, and J. Ahn, Opt. Lett. **35**, 508 (2010).
[17] F. Peter, S. Winnerl, S. Nitsche, A. Dreyhaupt, H. Schneider, and M. Helm, Appl. Phys. Lett. **91**, 081109 (2007).
[18] A. Nahata, A. S. Weling, and T. F. Heinz, Appl. Phys. Lett. **69**, 2321 (1996).
[19] K. Lee, J. Park, and J. Ahn (unpublished).
[20] X. F. Li, A. L'Huillier, M. Ferray, L. A. Lompre, and G. Mainfray, Phys. Rev. A **39**, 5751 (1989).
[21] P. Domachuk, N. A. Wolchover, M. Cronin-Golomb, A. Wang, A. K. George, C. M. B. Cordeiro, J. C. Knight, and F. G. Omenetto, Opt. Express **16**, 7161 (2008).